One year ozonesonde measurements at Kerguelen Island (49.2°S, 70.1°E): Influence of stratosphere-to-troposphere exchange and long-range transport of biomass burning plumes

Jean-Luc Baray, Valentin Duflot, Françoise Posny, Jean-Pierre Cammas, Anne M. Thompson, Franck Gabarrot, Jean-Louis Bonne, Guang Zeng

▶ **To cite this version:**

Jean-Luc Baray, Valentin Duflot, Françoise Posny, Jean-Pierre Cammas, Anne M. Thompson, et al.. One year ozonesonde measurements at Kerguelen Island (49.2°S, 70.1°E): Influence of stratosphere-to-troposphere exchange and long-range transport of biomass burning plumes. Journal of Geophysical Research: Atmospheres, 2012, 117 (D6), pp.D06305. 10.1029/2011JD016717 . hal-00961629

HAL Id: hal-00961629
https://hal.science/hal-00961629

Submitted on 15 Jun 2018

HAL is a multi-disciplinary open access archive for the deposit and dissemination of scientific research documents, whether they are published or not. The documents may come from teaching and research institutions in France or abroad, or from public or private research centers.

L'archive ouverte pluridisciplinaire **HAL**, est destinée au dépôt et à la diffusion de documents scientifiques de niveau recherche, publiés ou non, émanant des établissements d'enseignement et de recherche français ou étrangers, des laboratoires publics ou privés.

One year ozonesonde measurements at Kerguelen Island (49.2°S, 70.1°E): Influence of stratosphere-to-troposphere exchange and long-range transport of biomass burning plumes

Jean-Luc Baray,[1,2] Valentin Duflot,[1] Françoise Posny,[1,2] Jean-Pierre Cammas,[3] Anne M. Thompson,[4] Franck Gabarrot,[2] Jean-Louis Bonne,[1] and Guang Zeng[5]

Received 12 August 2011; revised 26 January 2012; accepted 27 January 2012; published 22 March 2012.

[1] We analyze a 1 year campaign of 17 ozonesondes launched in 2008–2009 at Kerguelen Island (49.2°S, 70.1°E), the first such soundings performed at this location. Tropospheric ozone presents a large variability in austral summer (December to February) and austral winter (June to September). The baseline tropospheric ozone is higher in winter (between 30 and 50 ppbv) than in summer (between 20 and 40 ppbv). We compare these observations to a data set obtained during the same period at Lauder (45.0°S, 169.7°E), which presents a marked seasonal pattern. The analysis of trajectory runs and reanalysis output help identify two significant contributors to the tropospheric ozone level at Kerguelen: the stratosphere-to-troposphere air mass transport and the long-range transport of biomass burning plumes. The stratosphere-to-troposphere transport is exemplified by a case study of a dry and enriched ozone layer over Kerguelen (70 ppbv at an altitude of 6 km on 28 February 2009). Using Lagrangian model simulations, we show that wintertime enhancement of the tropospheric ozone baseline can be partially attributed to the long-range transport of ozone precursors from biomass burning plumes originating in southern America and Africa. However, owing to limited data and to the many factors that can cause this wintertime baseline ozone enhancement, further investigations are needed to fully explain it. Additional measurements are also needed to establish an ozone climatology, to further characterize the ozone annual cycle and wintertime enhancement, and to better compare Kerguelen with other midlatitude sites.

Citation: Baray, J.-L., V. Duflot, F. Posny, J.-P. Cammas, A. M. Thompson, F. Gabarrot, J.-L. Bonne, and G. Zeng (2012), One year ozonesonde measurements at Kerguelen Island (49.2°S, 70.1°E): Influence of stratosphere-to-troposphere exchange and long-range transport of biomass burning plumes, *J. Geophys. Res.*, *117*, D06305, doi:10.1029/2011JD016717.

1. Introduction

[2] Ozone is a major greenhouse gas, whose radiative forcing depends on its vertical distribution between the stratosphere and the troposphere [*Lacis et al.*, 1990]. Understanding the climatological characteristics of tropospheric ozone production and fluxes at different temporal and spatial scales is thus important for assessing the direct effect of ozone on climate [*Pachauri et al.*, 2007]. Measurements of ozone profiles in the midlatitude Southern Hemisphere are sparse, in contrast to the Northern Hemisphere. Since 1998, fifteen stations have operated at various intervals in the Southern Hemisphere tropics and subtropics as part of the SHADOZ project (Southern Hemisphere Additional Ozonesondes, http://tropo.gsfc.nasa.gov/shadoz/) [*Thompson et al.*, 2003, 2011]. Recent studies based on SHADOZ data have demonstrated the role of biomass burning [*Diab et al.*, 2004; *Clain et al.*, 2009] and stratosphere-troposphere exchange [*Clain et al.*, 2010] on tropospheric ozone in the tropics and subtropics over Africa. These were complemented by Measurements of Ozone by In-Service Airbus Aircraft (MOZAIC) data [*Marenco et al.*, 1998], collected since 1994 and coupled with campaign ozonesondes performed in the framework of the African Monsoon Multidisciplinary Analysis (AMMA) experiment, allowing documentation of the tropospheric ozone production related to West African city emissions and the seasonal and interannual variability of ozone in both the troposphere and the lower stratosphere over West Africa [*Thouret et al.*, 2009; *Ancellet et al.*, 2011]. H. Morioka et al.

[1]Laboratoire de l'Atmosphère et des Cyclones, UMR 8105, Centre National de la Recherche Scientifique, Météo-France, Université de la Réunion, La Réunion, France.
[2]Unité Mixte de Service de l'OSU Réunion, UMS 3365, Centre National de la Recherche Scientifique, Université de la Réunion, La Réunion, France.
[3]Laboratoire d'Aérologie, UMR 5560, Centre National de la Recherche Scientifique, Université de Toulouse, Toulouse, France.
[4]Department of Meteorology, Pennsylvania State University, University Park, Pennsylvania, USA.
[5]National Institute of Water and Atmospheric Research, Lauder, New Zealand.

Published in 2012 by the American Geophysical Union.

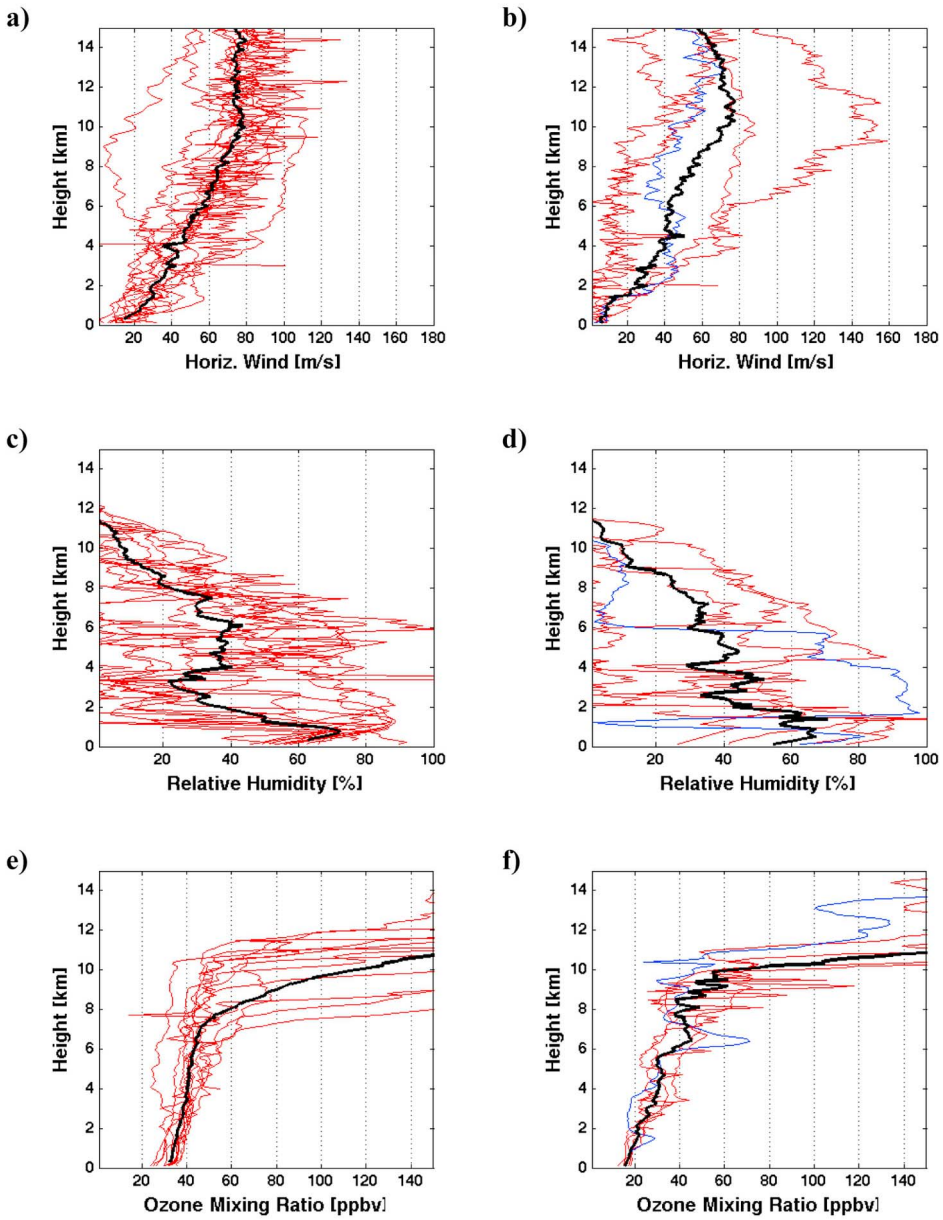

Figure 1. Profiles from austral winter (April to September 2008) and austral summer (December 2008 to February 2009) of (a and b) horizontal wind speed, (c and d) relative humidity, and (e and f) ozone mixing ratio, obtained from radiosondes over Kerguelen Island. The mean profiles are in black, and the radiosonde performed on 28 February 2009 is in blue.

(Interannual variations of ozone in the tropical troposphere and tropopause region from the SHADOZ and other ozonesonde data sets, Submitted to *Journal of Geophysical Research*, 2011) reported evidence of ozone increases in the upper troposphere over most SHADOZ stations.

[3] In midlatitude regions of the Southern Hemisphere, positive trends of tropospheric ozone have been analyzed by *Oltmans et al.* [2006], using long-term time series of tropospheric ozone profiles measured at different sites including Lauder (New Zealand, 45,0°S, 169,7°E). Measurement locations are sparse in these mainly oceanic regions. Observations from space platforms such as TOMS, SBUV or OMI, and more recently AIRS, TES or IASI cover tropospheric ozone over large areas, but with limited vertical resolution.

[4] In order to document midlatitude Southern Hemisphere ozone at a better vertical resolution, a one year ozonesonde campaign (part of ROCK project, Radiosondages Ozone Complémentaires aux Kerguelen) was undertaken from April 2008 to February 2009, at Kerguelen, a French oceanic archipelago at 49.2°S and 70.1°E in the Indian Ocean. In contrast to the Northern Hemisphere, the Southern Hemisphere is more oceanic and the troposphere is generally less polluted [*Fishman et al.*, 1990]. However, gaseous and aerosol products of biomass burning can be transported over

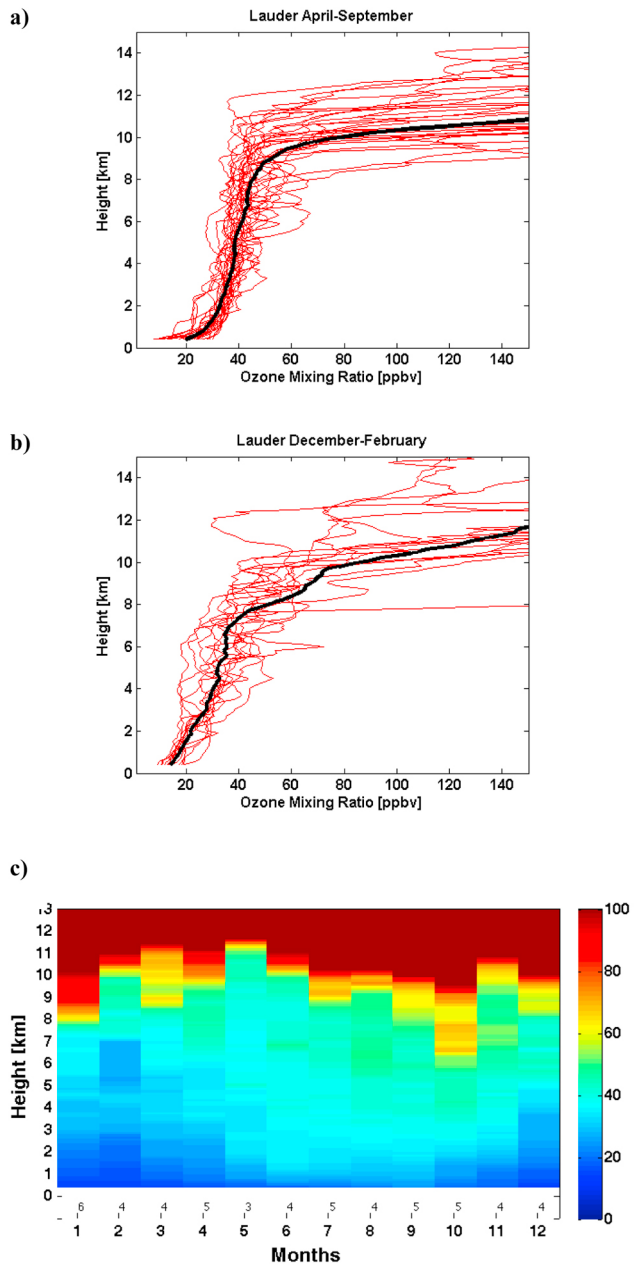

Figure 2. Ozone mixing ratio profiles over Lauder. (a) Profiles in austral winter, April to September 2008. (b) Profiles in austral summer, December 2008 to February 2009. (c) Monthly distribution of tropospheric ozone mixing ratio (0–100 ppbv) from April 2008 to March 2009. The number of individual profiles for each month is given just over the *x* axis.

long distances, with a significant impact on tropospheric trace gas composition [*Winkler et al.*, 2008]. The biomass burning season of the Southern Hemisphere occurs in austral winter and spring, and the Kerguelen archipelago is located in a major pathway fed by biomass burning from South America and southern Africa [*Edwards et al.*, 2006; *Duflot et al.*, 2010]. In addition, *Archer and Caldeira* [2008] showed that the jet stream is located near the latitude of Kerguelen, particularly in austral summer. This gives rise to stratosphere-to-troposphere transport over the site that can significantly influence the tropospheric ozone, the most extensive tropopause folding occurring in three-dimensional baroclinic developments associated with very strong jet streams [*Holton et al.*, 1995].

[5] The objective of this paper is to analyze the 2008–2009 Kerguelen ozonesonde data set. Since the number of measurements at Kerguelen is limited, we compare these observations to the tropospheric ozone seasonal variations observed over Lauder (45.0°S, 169.7°E), where ozonesondes have been routinely launched year-round since August 1986. Then, we document a stratosphere-to-troposphere-exchange event over Kerguelen and investigate the influence of biomass burning over this region.

2. Instrumental Setup and Tools

2.1. Instrumental Setup at Kerguelen and Lauder

[6] The balloon-borne sonde equipment used at Kerguelen is similar to that of Réunion Island, a SHADOZ and Network for the Detection of Atmospheric Composition Change (NDACC) station [*Baray et al.*, 2006]. It consists of a Z-ENSCI electrochemical concentration cell (ECC) that measures the ozone partial pressure profiles, coupled with a M2K2 Modem meteorological radiosonde to obtain temperature, relative humidity, GPS position and horizontal wind profiles. This type of meteorological sonde has been successfully used at the Réunion Island site since August 2007. Dual flights involving the previously used Vaisala RS80 and Modem M2K2 radiosonde system revealed no systematic bias and a better humidity estimation the Modem [*Posny et al.*, 2010]. The relative humidity measurements are with respect to water, and become physically meaningless above around 10 km, although they can provide qualitative information about cirrus clouds throughout the troposphere. Located in the roaring forties and close to the furious fifties, Kerguelen is exposed to almost continuous strong westerly winds and difficult weather conditions. Despite these, 12 balloons were successfully launched from April to September 2008 (16 April, 23 June, 29 June, 9 July, 22 July, 30 July, 23 August, 6 August, 11 August, 6 September, 19 September, and 27 September), and 5 from December 2008 to February 2009 (28 December, 18 January, 27 January, 16 February, and 28 February).

[7] The Lauder data set used in this study consists of 53 ozone profiles from 2 April 2008 to 23 March 2009, matching the Kerguelen experiment period. Two types of ozonesondes were launched with different radiosondes and interface cards (i.e., standard ozonesondes and those including a NOAA cryogenic water vapor instrument). Both used EN-SCI Z-series ECC ozone sensors operating with a 0.5% buffered KI cathode solution [*Boyd et al.*, 1998]. Radiosondes used were either a Vaisala RS92SGP with a Vaisala OIF-92 interface card (standard ozonesondes) or Vaisala RS80–15 with an ISD V2D interface card (NOAA water vapor sondes). Corrections are applied to the ozonesonde values above 200 hPa to account for pump efficiency degradation [*Bodeker et al.*, 1998; *Johnson et al.*, 2002]. The integrated ozone profile is compared to the total column of ozone measured by Dobson spectrophotometer at Lauder, and the discrepancy is typically less than 5% [*Bodeker et al.*, 1998].

Table 1. Ozone Mixing Ratio (ppbv) Averaged Over Each Site, Each Period, and 2 km Layers[a]

	Kerguelen			Lauder		
	June to September	December to February	JS-DF	June to September	December to February	JS-DF
Ground to 2 km	35.2 (2.9)	19.1 (2.5)	16.1	30.2 (2.8)	18.4 (3.8)	11.8
2–4 km	39.8 (3.2)	26.7 (5.5)	13.1	37.3 (2.9)	26.8 (5.4)	8.7
4–6 km	43.2 (4.7)	32.1 (5.2)	11.1	40.7 (4.3)	33.0 (8.8)	7.7
6–8 km	50.1 (13.1)	42.3 (9.1)	7.8	44.4 (6.6)	39.4 (12.1)	5.0
8–10 km	88.1 (58.9)	50.8 (15.8)	37.3	59.2 (25.5)	68.8 (52.5)	−9.6

[a]The standard deviation is given between brackets. The JS-DF columns give the difference between the two periods for each site.

2.2. Satellite Data

[8] The Moderate Resolution Imaging Spectroradiometer (MODIS) instrument on board the Terra and Aqua satellites (http://modis.gsfc.nasa.gov/) allows active fire detection based on the high infrared emissions of fires [*Giglio et al.*, 2003]. This information is available via the Fire Information for Resource Management System (FIRMS) site developed by the University of Maryland (http://maps.geog.umd.edu/firms/). FIRMS delivers active fires spots using the MODIS active fire locations processed by the MODIS Rapid Response System using the standard MODIS MOD14 Fire and Thermal Anomalies Product. Each active fire location represents the center of a 1 km × 1 km pixel that is flagged by the algorithm as containing a fire within the pixel.

2.3. Model Data

2.3.1. Meteorological Data

[9] The analysis of temperature, potential vorticity and winds presented in this paper are obtained from the European Centre for Medium-Range Weather Forecasts (ECMWF) ERA-Interim archive. The latitude/longitude resolution is 0.75° and the temporal resolution is 6 h (00:00, 06:00, 12:00, and 18:00 UT). The parameters are extracted on 37 pressure levels between 1 and 1000 hPa. ERA-Interim is an "interim" reanalysis of the period 1989 to the present in preparation for the next-generation extended reanalysis that will replace ERA-40. The main advances in the ERA-Interim data assimilation compared to ERA-40 are 12 h 4D-Var, T255 horizontal resolution, an improvement in the humidity analysis, model physics and data quality control, the variational bias correction of satellite radiance data, and other improvements in bias handling [*Dee and Uppala*, 2009; *Poli et al.*, 2010].

2.3.2. Trajectory Advection and Reverse Domain Filling Model

[10] Bundles of back trajectories have been computed using LACYTRAJ, a three-dimensional (i.e., kinematic) trajectory code using dynamical fields produced by the ECMWF. In this work we use ERA-Interim reanalysis. Each air parcel is advected using a linear interpolation of horizontal wind fields and time and a log linear interpolation for vertical wind field. This operation is done with a time step of 15 min in this work, for five days of back trajectories.

[11] The potential vorticity (PV) fields from meteorological analysis do not contain the fine-scale structures that can be reconstructed assuming PV conservation in the upper troposphere and lower stratosphere. Therefore, LACYTRAJ was also used to calculate vertical and horizontal distributions of PV with 48 h advection using the Reverse Domain Filling (RDF) trajectory mapping technique [*Sutton et al.*, 1994]. LACYTRAJ was previously used for climatology and case studies of stratosphere-troposphere exchange [*Clain et al.*, 2010; *Baray et al.*, 2010]. Our approach consists in advecting PV along back trajectories calculated on a regular gridded array so that mesoscale characteristics are enhanced by reconstruction of subgrid information that was not in the initial field [*Dritschel*, 1988].

[12] In addition we use FLEXPART version 8.2, which is a Lagrangian particle dispersion model [*Stohl et al.*, 2005] that simulates the transport and dispersion of linear tracers to evaluate the proportion of air masses coming from the stratosphere. FLEXPART treats advection and turbulent diffusion by processing the trajectories of a multitude number of particles. Stochastic fluctuations, obtained by solving Langevin equations [*Stohl and Thomson*, 1999], are superimposed on the grid-scale winds from the ECMWF data set to represent transport by turbulent eddies. FLEXPART is driven by global winds from ECMWF operational analysis and 3 h intermediate forecasts, with a horizontal resolution of 1 × 1 degree and 60 vertical levels, and a temporal resolution of 3 h.

[13] The Regional Real Time Fire Plumes (GIRAFE) model combines the MODIS fire count system with the FLEXPART Lagrangian model: at each fire pixel location detected by MODIS, a number of simulated particles are emitted and advected by the FLEXPART code [*Mari et al.*, 2008]. The 0.5° × 0.5° gridded fire counts are corrected for spatial variability in the frequency of satellite overpasses and missing observations. The particles were injected above fire pixels for 6 h. GIRAFE enables to choose between different types of emitted numerical particles having different physical properties (radioactivity, dry and wet deposition, etc.). In this set of simulations, the emitted pollutant is ozone. As recommended by *Dentener et al.* [2006], particles were uniformly emitted from the ground level up to 2000 m agl (above ground level) for each fire pixel detected by MODIS. Using this method, the GIRAFE model provides maps of a three-dimensional distribution of pollutants.

3. Observations of Tropospheric Ozone, Wind, and Humidity at Kerguelen

[14] Here we present the seasonal variation in the troposphere established from ozone radiosonde data obtained during the ROCK campaign. Profiles of horizontal wind, relative humidity, and ozone mixing ratio are shown in Figure 1. The data have been separated into two periods, one from December to February (referred to as "austral summer" in the following) and the other one from April to September (referred to as "austral winter" in the following; strictly speaking, it covers late autumn, winter and early spring).

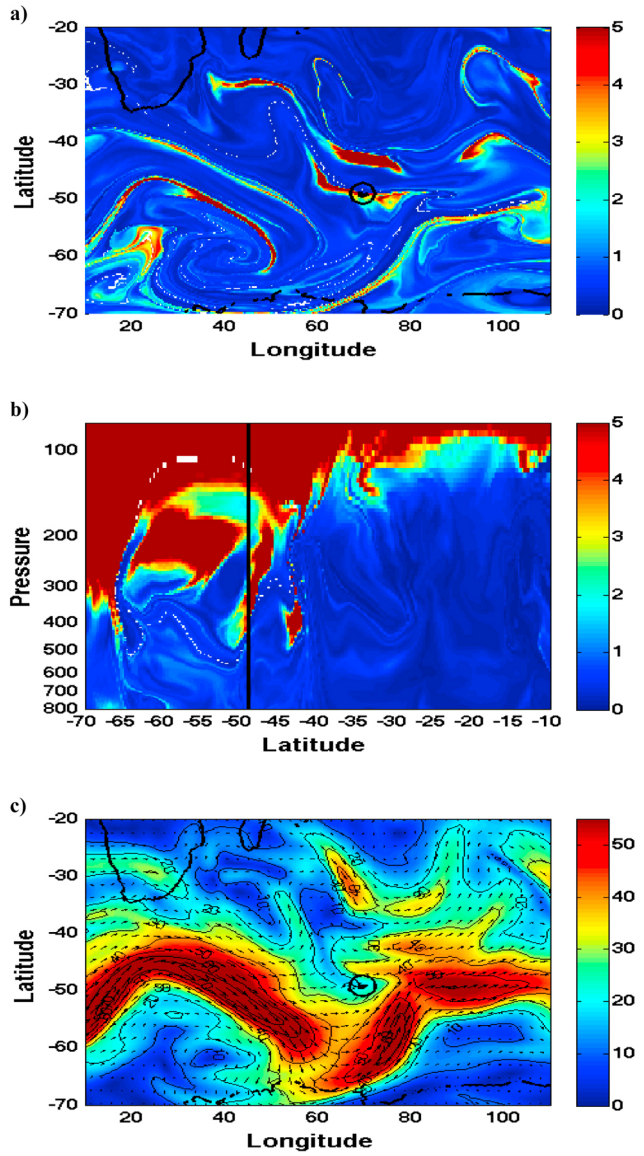

Figure 3. (a) Horizontal (at 400 hPa) distributions of advected potential vorticity and (b) vertical (at 70°E) distributions of advected potential vorticity, on 28 February 2009, 06:00 UT, calculated using the Reverse Domain Filling method applied on ECMWF ERA-Interim dynamical fields. (c) Horizontal wind at the pressure level 300 hPa on 28 February 2009, 06:00 UT (from ECMWF ERA-Interim dynamical fields). The wind speed is contoured along with wind vectors. The potential vorticity, negative in the Southern Hemisphere, is given in absolute values. The black circle and black lines locate the Kerguelen archipelago.

[15] The average surface wind maximizes during austral winter. It increases with altitude, reaching 80 m/s on average at 10 km, in austral winter and summer. The mean relative humidity profile shows large values in both austral winter and summer up to 8 km altitude.

[16] In April–September, tropospheric ozone ranges from 30 to 50 ppbv. There is no profile highly enriched in ozone, or with localized ozone layers. In austral summer, the values of ozone are lower (20–40 ppbv), but the profiles show more layering structures. As an example, the profile obtained on 28 February 2009 (in blue in Figure 1) presents a very dry and enriched ozone layer at 6 km. The typical altitude of the ozone tropopause defined by the increase of the ozone gradient varies from 8 to 12 km and from 10 to 12 km in austral winter and summer, respectively. Figures 1e and 1f show that the altitude of the ozone tropopause presents a large variability over Kerguelen, particularly in austral winter.

[17] The measurements at Kerguelen are too limited to display the tropospheric ozone seasonal variations at a monthly resolution. We thus compare the Kerguelen observations with the year-round vertical time series of tropospheric ozone over Lauder where the number of measurements is much larger (Figure 2). The ozone values for both Kerguelen and Lauder in June–September and December–February are given in Table 1. The ozone values are larger in June–September than in December–February from the ground to 10 km for Kerguelen and from the ground to 8km for Lauder. Taking into account of the standard deviations, the difference between the two periods maximizes from the ground to 6 km for Kerguelen and from the ground to 4 km for Lauder. The large variability observed over Kerguelen is also noted over Lauder for the two periods, where the ozone tropopause height varies also between 8 and 12 km (Figure 2); this could be associated with the proximity of the polar jet stream [*Archer and Caldeira*, 2008; *Holton et al.*, 1995].

[18] Over Kerguelen, the increase of ozone in austral winter (around + 20% compared to summer) evident in Figure 1 and Table 1 coincides with an ozone enhancement in the free and upper troposphere observed over Lauder from June to November (Figure 2) and is consistent with TOMS/SAGE and SBUV satellite observations [*Fishman et al.*, 2003] and MOZART 2 model simulations [*Horowitz et al.*, 2003]. This is also consistent with the work of *Clain et al.* [2009], who showed an ozone cycle for two sites of the Southern Hemisphere subtropics (Irene, South Africa, 26°S and Réunion Island, 21°S), with a maximum in spring corresponding to the biomass burning season. However, additional measurements are needed to establish a Kerguelen ozone climatology, to characterize the ozone annual cycle, and to investigate possible local peculiarities in comparison with Lauder.

4. Discussion

4.1. Examination of the 28 February Case Study

[19] Tropospheric ozone variability in the tropics and subtropics can be produced by photochemical production [*Chatfield and Delany*, 1990; *Thompson et al.*, 1996, 1997; *Chatfield et al.*, 2007; *Folkins et al.*, 2000], or by stratospheric intrusion into the troposphere [*Holton et al.*, 1995]. A dry and enriched ozone layer reaching 70 ppbv at 6 km was identified on 28 February 2009.

[20] The synoptic situation associated with observations of this ozonesonde is analyzed using ECMWF data (Figure 3). The analysis of tropopause height using the ECMWF ERA-Interim 1.5 PVU surface reveals that a stratospheric filament passed over Kerguelen Island on 28 February between 00:00 and 06:00 UTC (not shown). The horizontal range of this filament is larger than 1000 km. In order to investigate the fine-scale structure of this filament, cross sections of

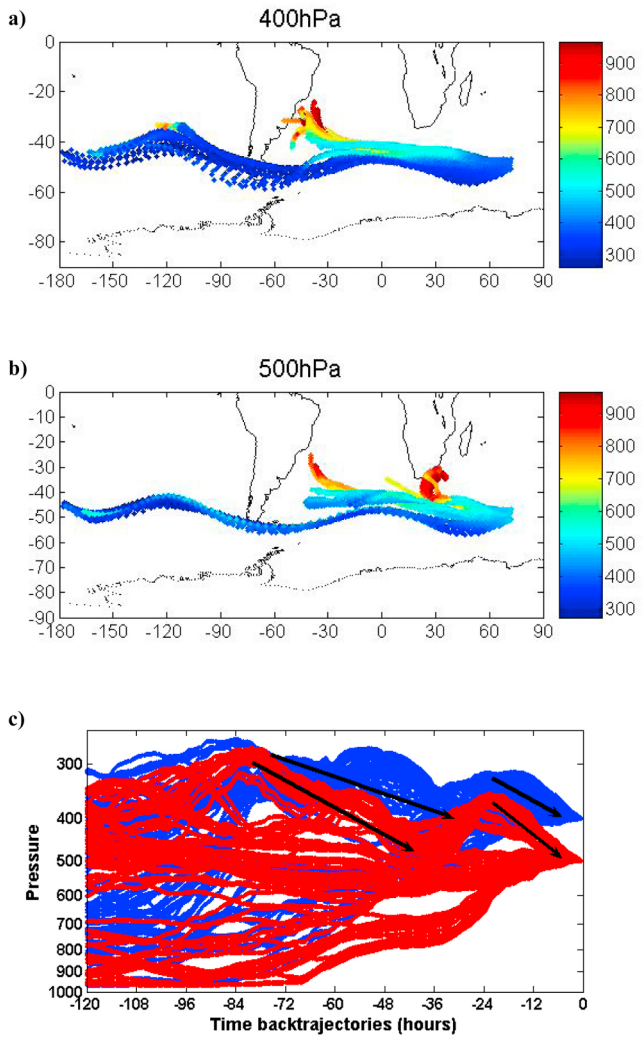

Figure 4. LACYTRAJ back trajectories of air masses ending over Kerguelen Island at (a) 400 hPa and (b) 500 hPa, on 28 February 2009, 06:00 UT; the color scale indicates the pressure level of the air masses. (c) The pressure level of air masses given as a function of time before 28 February 2009, 06:00 UT. The clusters ending at 400 and 500 hPa are in blue and red, respectively; black arrows highlight the subsidence of air masses.

advected potential vorticity were calculated using the Reverse Domain Filling method. Figures 3a and 3b indicate that the value of advected PV inside the filament on 28 February 2009 at 06:00 UT exceeds 3 PVU and that the vertical structure of the stratospheric-origin filament extends from 300 to 400 hPa, corresponding to the altitudes of 6 and 9 km. This is in good agreement with the altitude of the ozone peak identified in the ozone profile (Figure 1f).

[21] This intrusion was associated with Rossby wave breaking event, with the formation of multiple stratospheric filaments, and the polar jet stream formed a waveshape (Figure 3c). This undulatory structure is also revealed by LACYTRAJ bundles of back trajectories (Figure 4). The bundles of back trajectories reveal that the air mass arriving over Kerguelen at the 400 and 500 hPa levels is a mixture of air masses from different origins: some are near the surface (South America for the 400 hPa bundle and both South America and Africa for the 500 hPa bundle), the remainder is in the midlatitude stratosphere. The movement of air masses in the vertical plane (Figure 4c) shows that the subsiding part of the cluster took place in two steps, the older one between 84 to 36 h before arriving over Kerguelen, and the younger one within 24 h before arriving over Kerguelen. The end of the older subsidence, 36 h before arriving over Kerguelen (i.e., on 26 February 2009, 18:00 UTC), corresponds to a location near 0 degree of longitude and between 40 and 50°S.

[22] The ECMWF ERA-Interim vertical cross sections, for this longitude and time, of PV and relative humidity (Figure 5), reveal a stratospheric intrusion reaching the 550 hPa pressure level near 45 degrees south. We conclude that the tropospheric ozone peak observed at 6 km at Kerguelen on 28 February is a mixing of tropospheric and stratospheric air masses, arriving over Kerguelen after two successive subsidences. Ozone observed over Kerguelen (70 ppbv) can be low despite large absolute ECMWF ERA-Interim PV. Observations of various dynamical events of stratosphere-to-troposphere exchange over other areas present frequently exhibit more ozone. As an example, *Roelofs et al.* [2003] observed a layer between 80 and 120 ppbv and of 2 km thickness over Europe. *Scott et al.* [2001] analyzed filamentation induced by Rossby Wave breaking over the South Atlantic and found that ozone in the filaments exceeded 90 ppbv. *Jing et al.* [2005] observed more than 110 ppbv in the upper troposphere over Japan, and *Kowol-Santen and Ancellet* [2000] observed more than

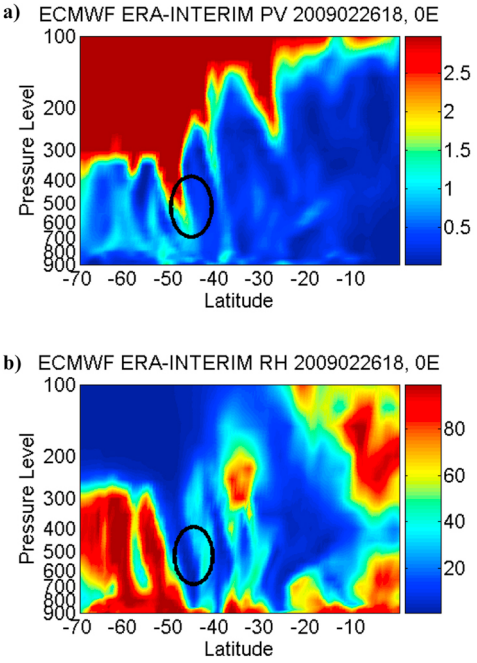

Figure 5. Vertical distributions of (a) potential vorticity (PV) and (b) relative humidity (RH), from ECMWF ERA-Interim dynamical fields on 26 February 2009, 18:00 UT, at 0° of longitude, corresponding to time and location of the older subsidence seen by LACYTRAJ back trajectories. The black ellipses highlight the stratospheric intrusion.

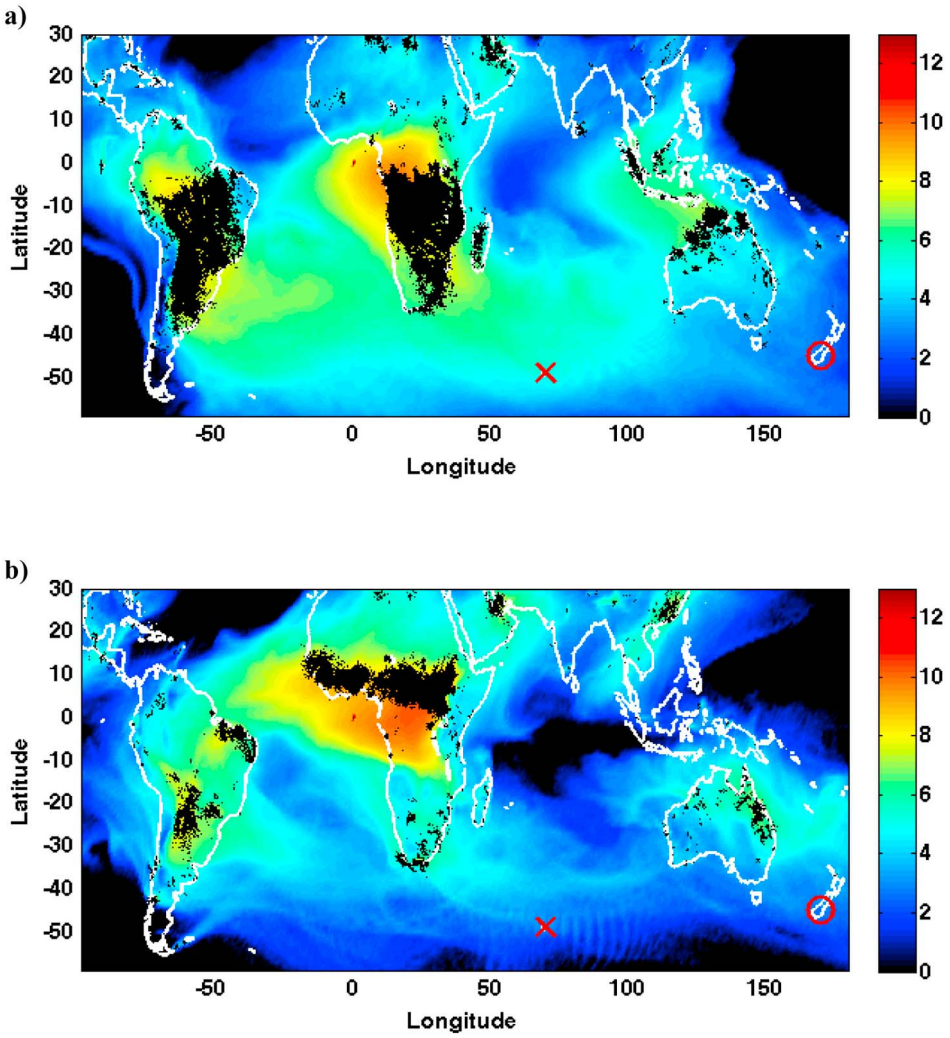

Figure 6. Geographical distribution of 1° × 1° averaged particles (arbitrary unit) for 7 days GIRAFE simulations from (a) 1 June to 30 September 2008 (winter) and (b) 1 December 2008 to 28 February 2009 (summer). Black dots are fires detected by MODIS. The red crosses and red circles locate the Kerguelen archipelago and Lauder, respectively.

200 ppbv over the North Atlantic Ocean with airborne lidar measurements.

[23] We perform FLEXPART calculations to evaluate the ratio of stratosphere-to-troposphere-origin air masses. The back trajectories (not shown) are calculated by initializing particles from a box bounded by 48°S and 46.5°S, 66°E and 78°E, respectively, and 350 hPa and 300 hPa. This region corresponds to the nearest part of the filament to Kerguelen, where PV from the ERA-Interim reanalysis is higher than 1.5 PVU. The observed ozone peak originates from a mixing of two air masses and is composed of ~25% of stratospheric air masses. This ratio is to be considered carefully, since it depends sensitively on poorly quantified ERA-Interim vertical velocities. However, it is consistent with a somewhat lower ozone amount than other examples of stratosphere-troposphere exchange published previously [*Kowol-Santen and Ancellet*, 2000; *Baray et al.*, 2003].

4.2. Origin of the Seasonal Ozone Maximum During Winter

[24] Figure 2 shows that for both sites the baseline ozone is higher in austral winter (30–50 ppbv) than in austral summer (20–40 ppbv). Such greater abundance in austral winter can be caused by a change in the background tropospheric chemistry, by more stratosphere-troposphere exchange (STE) in winter than in summer and by the photochemical production of ozone from biomass burning ozone precursors [*Stevenson et al.*, 2006] that are transported toward the Kerguelen archipelago and New Zealand. *Hauglustaine et al.* [1999] analyzed the tropospheric photochemical cycles above Mauna Loa (19°N, 155°W) and showed that at Hawaii, throughout the year production and destruction of ozone are in quasi-equilibrium in the free troposphere. Since Kerguelen and Lauder are both mostly background sites, the increased tropospheric ozone background in winter is likely not caused by a change in the tropospheric background photochemistry.

Table 2. Biomass Burning Tracer Loading (Arbitrary Unit) Calculated With the GIRAFE Model, Averaged Over Each Site, Each Period, and 2 km Layers[a]

	Kerguelen			Lauder		
	June to September	December to February	JS-DF	June to September	December to February	JS-DF
Ground to 2 km	3.58 (2.83)	0.11 (0.06)	3.47	1.91 (1.26)	0.60 (1.04)	1.31
2–4 km	14.33 (10.76)	0.77 (0.62)	13.56	2.54 (2.71)	1.12 (1.79)	1.42
4–6 km	45.83 (61.65)	4.78 (4.44)	41.05	2.36 (1.33)	1.76 (1.96)	0.60
6–8 km	43.17 (41.43)	5.46 (5.29)	37.71	2.82 (3.03)	3.42 (3.71)	−0.60
8–10 km	44.19 (46.40)	2.27 (1.91)	41.92	2.29 (2.72)	3.30 (3.37)	−1.01

[a]The standard deviation is given between brackets. The JS-DF columns give the difference between the two periods for each site.

Appenzeller et al. [1996] examined the annual cycle of the net mass transport across the extratropical tropopause and showed a maximum of net downward mass transport in winter for the Southern Hemisphere. Thus, the absence of layers in the wintertime Kerguelen profiles and of marked stratosphere-to-troposphere transport using ERA-Interim reanalysis does not totally rule out the stratosphere-to-troposphere transport hypothesis, this requires investigation. Rather, here, we assess the hypothesis that biomass burning causes the observed increase of ozone by performing a set of simulations using the GIRAFE-FLEXPART model (section 2.3.2).

[25] Seven day forward GIRAFE-FLEXPART simulations were performed for each day from 1 June to 30 September 2008 in winter and from 1 December 2008 to 28 February 2009 in summer. Particles were emitted up to 2000 m agl (section 2.3.2) for each fire pixel detected by MODIS (section 2.3.1). Figure 6 shows the probability density function of the emitted particles resulting from this set of simulations. Note that the geographical distributions are integrated over the entire troposphere. Biomass burning activity is clearly higher in austral winter (Figure 6a) than in austral summer (Figure 6b), and the plumes emitted by the biomass burning activity, containing ozone precursors and enhanced ozone from southern Africa and South America are transported toward the Kerguelen archipelago during both periods. This is consistent with studies showing that the Kerguelen archipelago is located in the transport pathway from South America and southern Africa to Australia [*Edwards et al.*, 2006; *Duflot et al.*, 2010]. While Kerguelen is clearly more affected by transport of biomass burning plumes during austral winter than during austral summer, Lauder exhibits a relatively invariant loading throughout both periods (∼2 AU, arbitrary unit). It seems therefore that Lauder may be more influenced by biomass burning plumes emitted from Australian fires during both periods than by those emitted from Southern Africa and South America. Indeed, fire activity occurs in Australia from September to January [*Van der Werf et al.*, 2006] and thus impacts Lauder during both periods.

[26] Table 2 shows the biomass burning tracer loading for each 2 km thick layer, each site and each period. For both sites, the main loading occurs above 2 km, and is greater in austral winter than in austral summer, except for Lauder above 6 km, in good accordance with the observations (Table 1) as well as with previous studies of southern African burning and export [*Thompson et al.*, 1996; *Oltmans et al.*, 2001; *Swap et al.*, 2002; *Thompson et al.*, 2002]. However, the simulated biomass burning tracer enhancement above Kerguelen between austral summer and winter (around 1 order of magnitude) is much greater than the observed ozone enhancement (Table 1), which is not the case for Lauder. The following model limitations should be taken into consideration when considering the resulting simulations: (1) the simulations only deal with the biomass burning source (neither anthropogenic nor STE sources); (2) the same number of particles was emitted from each fire, irrespective of the type of biomass burnt; (3) emitted particles were uniformly distributed in altitude and emitted at the same injection height (2 km agl), independently from the location of the fire; (4) the processes affecting the ozone production from precursors were not taken into account; and (5) the ozone production rate from precursors depends on photochemical conditions; so, the simulated biomass burning tracer enhancement may not be directly related to the ozone one.

[27] Despite these limitations, this set of simulations confirms that the higher baseline of tropospheric ozone over the Kerguelen archipelago is partially due to the higher biomass burning activity occurring in Southern Africa and South America during austral winter. Further studies will be necessary to quantitatively investigate the roles of biomass burning and STE on the ozone background seasonality.

[28] To assess the relative contribution of South American and Southern African biomass burning activities to the austral winter baseline ozone in Kerguelen, we perform the winter simulations (from 1 June to 30 September 2008) separately for each of these two areas and counted the number of particles passing over Kerguelen during the whole period. The resulting relative winter contributions are: 57% from South America and 43% from Southern Africa. Although this last result might mean that the contribution from long-range transport of fire emissions from South America is a bit stronger compared to the one associated with South Africa fires over the observation site, the respective contributions to ozone production will have to be assessed with a chemistry-transport model that can more accurately take into account differences in age of air masses and fire characteristics.

5. Conclusion

[29] The objective of this paper is to analyze a 1 year campaign of seventeen ozonesondes at Kerguelen (49.2°S; 70.1°E), the first performed at this location. We have presented the main characteristics of tropospheric ozone at this location, as well as wind, and humidity. The measurements at Kerguelen show that the baseline ozone is more elevated in winter than in summer, but additional measurements are needed to characterize the ozone annual cycle.

[30] An enlightening example of summertime stratosphere-to-troposphere exchange is identified for 28 February 2009. The case study is based on global reanalyses and Lagrangian simulations. It shows evidence of the intrusion of a stratospheric filament into the troposphere that is associated with a perturbed polar jet stream, and is mixed with tropospheric tropical air masses. We used the GIRAFE-FLEXPART model to show that one of the causes of the higher baseline ozone in winter than in summer might be the stronger biomass burning activity occurring in southern Africa and South America in austral winter, and by transport of the emitted plumes toward the Kerguelen archipelago. However, the wintertime additional contribution of stratosphere-troposphere exchange to this higher ozone baseline cannot be excluded. It would be interesting to continue this ozonesonde measurement series at Kerguelen because this data set appears exceptionally rich and promising for stratospheric and tropospheric studies. Measurements throughout a year would allow better characterization of an annual ozone cycle.

[31] **Acknowledgments.** The Laboratoire de l'Atmosphère et des Cyclones (LACY) is a laboratory of the University of Réunion Island associated with CNRS-INSU (Institut National des Sciences de l'Univers) and Météo-France. The present work has been conducted in the framework of the ROCK program supported by the program 109 of the Institut polaire Paul Emile Victor (IPEV) and by the regional council of Réunion Island. We are grateful to the Météo-France radiosonde team at Kerguelen for having carried out the balloon launches during the campaign. The Lauder ozonesonde measurement is funded by the New Zealand Foundation for Research Science and Technology. We acknowledge Hamish Chisholm and Alan Thomas, who carried out these measurements. We acknowledge ECMWF for providing ERA-Interim reanalysis. We acknowledge the MODIS mission scientists and associated NASA personnel, as well as the Giovanni online data system, developed and maintained by the NASA GES DISC, for providing MODIS AOT data. GIRAFE is supported by ETHER (CNES and INSU-CNRS). We also thank the University of Maryland for providing fires detection data.

References

Ancellet, G., E. Orlandi, E. Real, K. S. Law, H. Schlager, F. Fierli, J. K. Nielsen, V. Thouret, and C. Mari (2011), Tropospheric ozone production related to West African city emissions during the 2006 wet season AMMA campaign, *Atmos. Chem. Phys.*, *11*, 6349–6366, doi:10.5194/acp-11-6349-2011.

Appenzeller, C., J. R. Holton, and K. H. Rosenlof (1996), Seasonal variation of mass transport across the tropopause, *J. Geophys. Res.*, *101*, 15,071–15,078.

Archer, C. L., and K. Caldeira (2008), Historical trends in the jet streams, *Geophys. Res. Lett.*, *35*, L08803, doi:10.1029/2008GL033614.

Baray, J. L., S. Baldy, R. D. Diab, and J. P. Cammas (2003), Dynamical study of a tropical cut-off low over South Africa, and its impact on tropospheric ozone, *Atmos. Environ.*, *37*, 1475–1488, doi:10.1016/S1352-2310(02)00999-8.

Baray, J. L., et al. (2006), An instrumented station for the survey of ozone and climate change in the southern tropics: Scientific motivation, technical description and future plans, *J. Environ. Monit.*, *8*, 1020–1028, doi:10.1039/B607762E.

Baray, J. L., G. Clain, M. Plu, E. Feld, and P. Caroff (2010), Occurrence of monsoon depressions in the Southwest Indian Ocean: Synoptic descriptions and stratosphere to troposphere exchange investigations, *J. Geophys. Res.*, *115*, D17108, doi:10.1029/2009JD013390.

Bodeker, G. E., I. S. Boyd, and W. A. Matthews (1998), Trends and variability in vertical ozone and temperature profiles measured by ozonesondes at Lauder, New Zealand: 1986–1996, *J. Geophys. Res.*, *103*, 28,661–28,681, doi:10.1029/98JD02581.

Boyd, I. S., G. E. Bodeker, B. J. Connor, D. P. J. Swart, and E. J. Brinksma (1998), An assessment of ECC ozonesondes operated using 1% and 0.5% KI cathode solutions at Lauder, New Zealand, *Geophys. Res. Lett.*, *25*, 2409–2412, doi:10.1029/98GL01814.

Chatfield, R. B., and A. C. Delany (1990), Convection links biomass burning to increased tropical ozone: However, models will tend to overpredict O_3, *J. Geophys. Res.*, *95*, 18,473–18,488, doi:10.1029/JD095iD11p18473.

Chatfield, R. B., H. Guan, A. M. Thompson, and H. G. J. Smit (2007), Mechanisms for the intraseasonal variability of tropospheric ozone over the Indian Ocean during the winter monsoon, *J. Geophys. Res.*, *112*, D10303, doi:10.1029/2006JD007347.

Clain, G., J. L. Baray, R. Delmas, R. Diab, J. Leclair de Bellevue, P. Keckhut, F. Posny, J. M. Metzger, and J. P. Cammas (2009), Tropospheric ozone climatology at two Southern Hemisphere tropical/subtropical sites (Reunion Island and Irene, South Africa) from ozonesondes, LIDAR, and in situ aircraft measurements, *Atmos. Chem. Phys.*, *9*, 1723–1734, doi:10.5194/acp-9-1723-2009.

Clain, G., J. L. Baray, R. Delmas, P. Keckhut, and J.-P. Cammas (2010), A lagrangian approach to analyse the tropospheric ozone climatology in the tropics: Climatology of stratosphere-troposphere exchange at Reunion Island, *Atmos. Environ.*, *44*, 968–975, doi:10.1016/j.atmosenv.2009.08.048.

Dee, D. P., and S. Uppala (2009), Variational bias correction of satellite radiance data in the ERA-Interim reanalysis, *Q. J. R. Meteorol. Soc.*, *135*, 1830–1841, doi:10.1002/qj.493.

Dentener, F., et al. (2006), Emissions of primary aerosol and precursor gases in the years 2000 and 1750 prescribed data-sets for AeroCom, *Atmos. Chem. Phys.*, *6*, 4321–4344, doi:10.5194/acp-6-4321-2006.

Diab, R. D., A. M. Thompson, K. Mari, L. Ramsay, and G. J. R. Coetzee (2004), Tropospheric ozone climatology over Irene, South Africa, from 1990 to 1994 and 1998 to 2002, *J. Geophys. Res.*, *109*, D20301, doi:10.1029/2004JD004793.

Dritschel, D. G. (1988), A topological reconnection scheme for extended integrations using contour dynamics, *J. Comput. Phys.*, *77*, 240–266, doi:10.1016/0021-9991(88)90165-9.

Duflot, V., B. Dils, J. L. Baray, M. De Mazière, J. L. Attié, G. Vanhaelewyn, C. Senten, C. Vigouroux, G. Clain, and R. Delmas (2010), Analysis of the origin of the distribution of CO in the subtropical southern Indian Ocean in 2007, *J. Geophys. Res.*, *115*, D22106, doi:10.1029/2010JD013994.

Edwards, D. P., et al. (2006), Satellite-observed pollution from Southern Hemisphere biomass burning, *J. Geophys. Res.*, *111*, D14312, doi:10.1029/2005JD006655.

Fishman, J., C. E. Watson, J. C. Larsen, and J. A. Logan (1990), Distribution of tropospheric ozone determined from satellite data, *J. Geophys. Res.*, *95*, 3599–3617, doi:10.1029/JD095iD04p03599.

Fishman, J., A. E. Wozniak, and J. K. Creilson (2003), Global distribution of tropospheric ozone from satellite measurements using the empirically corrected tropospheric ozone residual technique: Identification of the regional aspects of air pollution, *Atmos. Chem. Phys.*, *3*, 893–907, doi:10.5194/acp-3-893-2003.

Folkins, I., S. J. Oltmans, and A. M. Thompson (2000), Tropical convective outflow and near-surface equivalent potential temperatures, *Geophys. Res. Lett.*, *27*, 2549–2552, doi:10.1029/2000GL011524.

Giglio, L., et al. (2003), An enhanced contextual fire detection algorithm for MODIS, *Remote Sens. Environ.*, *87*, 273–282, doi:10.1016/S0034-4257(03)00184-6.

Hauglustaine, D. A., S. Madronich, B. A. Ridley, S. J. Flocke, C. A. Cantrell, F. L. Eisele, R. E. Shetter, D. J. Tanner, P. Ginoux, and E. L. Atlas (1999), Photochemistry and budget of ozone during the Mauna Loa Observatory Photochemistry Experiment (MLOPEX 2), *J. Geophys. Res.*, *104*, 30,275–30,307, doi:10.1029/1999JD900441.

Holton, J. R., P. H. Haynes, M. E. McIntyre, A. R. Douglass, R. B. Rood, and L. Pfister (1995), Stratosphere-troposphere exchange, *Rev. Geophys.*, *33*, 403–439, doi:10.1029/95RG02097.

Horowitz, L. W., et al. (2003), A global simulation of tropospheric ozone and related tracers: Description and evaluation of MOZART, version 2, *J. Geophys. Res.*, *108*(D24), 4784, doi:10.1029/2002JD002853.

Jing, P., D. M. Cunnold, E.-S. Yang, and H.-J. Wang (2005), Influence of isentropic transport on seasonal ozone variations in the lower stratosphere and subtropical upper troposphere, *J. Geophys. Res.*, *110*, D10110, doi:10.1029/2004JD005416.

Johnson, B. J., S. J. Oltmans, H. Vömel, H. G. J. Smit, T. Deshler, and C. Kröger (2002), Electrochemical concentration cell (ECC) ozonesonde pump efficiency measurements and tests on the sensitivity to ozone of buffered and unbuffered ECC sensor cathode solutions, *J. Geophys. Res.*, *107*(D19), 4393, doi:10.1029/2001JD000557.

Kowol-Santen, J., and G. Ancellet (2000), Mesoscale analysis of transport across the subtropical tropopause, *Geophys. Res. Lett.*, *27*, 3345–3348, doi:10.1029/2000GL011369.

Lacis, A. A., D. J. Wuebbles, and J. A. Logan (1990), Radiative forcing of climate by changes in the vertical distribution of ozone, *J. Geophys. Res.*, *95*, 9971–9981, doi:10.1029/JD095iD07p09971.

Marenco, A., et al. (1998), Measurement of ozone and water vapor by Airbus in-service aircraft: The MOZAIC airborne program, An overview, *J. Geophys. Res.*, *103*, 25,631–25,642, doi:10.1029/98JD00977.

Mari, C. H., G. Cailley, L. Corre, M. Saunois, J. L. Attié, V. Thouret, and A. Stohl (2008), Tracing biomass burning plumes from the Southern Hemisphere during the AMMA 2006 wet season experiment, *Atmos. Chem. Phys.*, *8*, 3951–3961, doi:10.5194/acp-8-3951-2008.

Oltmans, S. J., et al. (2001), Ozone in the Pacific tropical troposphere from ozonesonde observations, *J. Geophys. Res.*, *106*, 32,503–32,525, doi:10.1029/2000JD900834.

Oltmans, S. J., et al. (2006), Long-term changes in tropospheric ozone, *Atmos. Environ.*, *40*, 3156–3173, doi:10.1016/j.atmosenv.2006.01.029.

Pachauri, R. K., et al. (2007), *Climate Change 2007: Synthesis Report, Contribution of Working Groups I, II and III to the Fourth Assessment Report of the Intergovernmental Panel on Climate Change*, 104 pp., Intergovernmental Panel on Climate Change, Geneva, Switzerland.

Poli, P., S. B. Healy, and D. P. Dee (2010), Assimilation of Global Positioning System radio occultation data in the ECMWF ERA-Interim reanalysis, *Q. J. R. Meteorol. Soc.*, *136*, 1972–1990, doi:10.1002/qj.722.

Posny, F., J. M. Metzger, and J. L. Baray (2010), A successful change at La Réunion Island Station (21°S, 55.5°E), *SHADOZ Newsl.*, *11*, 3.

Roelofs, G. J., et al. (2003), Intercomparison of tropospheric ozone models: Ozone transport in a complex tropopause folding event, *J. Geophys. Res.*, *108*(D12), 8529, doi:10.1029/2003JD003462.

Scott, R. K., J.-P. Cammas, P. Mascart, and C. Stolle (2001), Stratospheric filamentation into the upper tropical troposphere, *J. Geophys. Res.*, *106*, 11,835–11,848, doi:10.1029/2001JD900049.

Stevenson, D. S., et al. (2006), Multimodel ensemble simulations of present-day and near-future tropospheric ozone, *J. Geophys. Res.*, *111*, D08301, doi:10.1029/2005JD006338.

Stohl, A., and D. J. Thomson (1999), A density correction for Lagrangian particle dispersion models, *Boundary Layer Meteorol.*, *90*(1), 155–167, doi:10.1023/A:1001741110696.

Stohl, A., et al. (2005), Technical note: The Lagrangian particle dispersion model FLEXPART version 6.2, *Atmos. Chem. Phys.*, *5*, 2461–2474, doi:10.5194/acp-5-2461-2005.

Sutton, R. T., H. Maclean, R. Swinbank, A. O'Neill, and F. W. Taylor (1994), High-resolution stratospheric tracer fields estimated from satellite observations using Lagrangian trajectory calculations, *J. Atmos. Sci.*, *51*, 2995–3005, doi:10.1175/1520-0469(1994)051<2995:HRSTFE>2.0.CO;2.

Swap, R. J., et al. (2002), The Southern African Regional Science Initiative (SAFARI-2000): Dry-season campaign, an overview, *S. Afr. J. Sci.*, *98*, 125–130.

Thompson, A. M., K. E. Pickering, D. P. McNamara, M. R. Schoeberl, R. D. Hudson, J. H. Kim, E. V. Browell, V. W. J. H. Kirchhoff, and D. Nganga (1996), Where did tropospheric ozone over southern Africa and the tropical Atlantic come from in October 1992? Insights from TOMS, GTE/TRACE-A, and SAFARI-92, *J. Geophys. Res.*, *101*, 24,251–24,278, doi:10.1029/96JD01463.

Thompson, A. M., W.-K. Tao, K. E. Pickering, J. R. Scala, and J. Simpson (1997), Tropical deep convection and ozone formation, *Bull. Am. Meteorol. Soc.*, *78*, 1,043–1,054.

Thompson, A. M., J. C. Witte, M. T. Freiman, N. A. Phahlane, and G. J. R. Coetzee (2002), Lusaka, Zambia, during SAFARI-2000: Convergence of local and imported ozone pollution, *Geophys. Res. Lett.*, *29*(20), 1976, doi:10.1029/2002GL015399.

Thompson, A. M., et al. (2003), Southern Hemisphere Additional Ozonesondes (SHADOZ) 1998–2000 tropical ozone climatology: 1. Comparison with Total Ozone Mapping Spectrometer (TOMS) and ground-based measurements, *J. Geophys. Res.*, *108*(D2), 8238, doi:10.1029/2001JD000967.

Thompson, A. M., S. J. Oltmans, D. W. Tarasick, P. von der Gathen, H. G. J. Smit, and J. C. Witte (2011), Strategic ozone sounding networks: Review of design and accomplishments, *Atmos. Environ.*, *45*, 2145–2163.

Thouret, V., et al. (2009), An overview of two years of ozone radio soundings over Cotonou as part of AMMA, *Atmos. Chem. Phys.*, *9*, 6157–6174, doi:10.5194/acp-9-6157-2009.

Van der Werf, G. R., J. T. Randerson, L. Giglio, G. J. Collatz, and P. S. Kasibhatla (2006), Interannual variability in global biomass burning emission from 1997 to 2004, *Atmos. Chem. Phys.*, *6*, 3423–3441, doi:10.5194/acp-6-3423-2006.

Winkler, H., P. Formenti, D. J. Esterhuyse, R. J. Swap, G. Helas, H. J. Annegarn, and M. O. Andreae (2008), Evidence for large-scale transport of biomass burning aerosols from sunphotometry at a remote South African site, *Atmos. Environ.*, *42*, 5569–5578, doi:10.1016/j.atmosenv.2008.03.031.

J.-L. Baray, J.-L. Bonne, V. Duflot, and F. Posny, Laboratoire de l'Atmosphère et des Cyclones, UMR 8105, Centre National de la Recherche Scientifique, Météo-France, Université de la Réunion, F-97715 Saint-Denis CEDEX 9, La Réunion, France. (barray@univ-reunion.fr)

J.-P. Cammas, Laboratoire d'Aérologie, UMR 5560, Centre National de la Recherche Scientifique, Université de Toulouse, F-31400 Toulouse, France.

F. Gabarrot, Unité Mixte de Service de l'OSU Réunion, UMS 3365, Centre National de la Recherche Scientifique, Université de la Réunion, F-97715 Saint-Denis CEDEX 9, La Réunion, France.

A. M. Thompson, Department of Meteorology, Pennsylvania State University, College Park, PA 16802, USA.

G. Zeng, National Institute of Water and Atmospheric Research, Private Bag 50061, Lauder 1149, New Zealand.